Supporting Information

Cobaloxime Anchored MoS_2 Nanosheets as Electrocatalysts for Hydrogen Evolution Reaction

Ming Cai,[a] Fan Zhang,[a] Chao Zhang,[a] Chenbao Lu,[a] Yafei He,[a] Yang Qu,[b] Hao Tian,[a] Xinliang Feng,[c] Xiaodong Zhuang*[ac]*

[a] State Key Laboratory of Metal Matrix Composites, Shanghai Key Laboratory of Electrical Insulation and Thermal Ageing, School of Chemistry and Chemical Engineering, Shanghai Jiao Tong University, 200240 Shanghai, P. R. China
E-mail: fan-zhang@sjtu.edu.cn; zhuang@sjtu.edu.cn
[b] School of Electronic Information and Electrical Engineering, Shanghai Jiao Tong University 200240 Shanghai, P. R. China.
[c] Center for Advancing Electronics Dresden & Department of Chemistry and Food Chemistry, Technische Universität Dresden, 01062 Dresden, Germany.

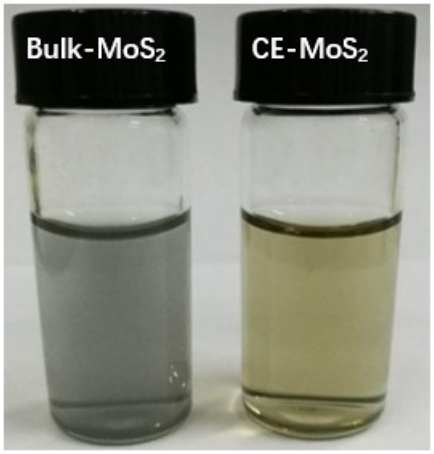

Figure S1. Photography of bulk MoS_2 and CE-MoS_2 dispersions in deionized water.

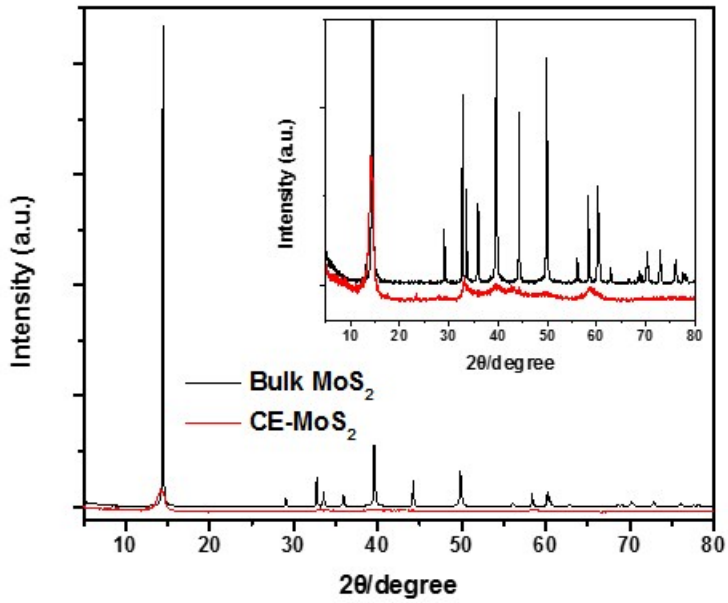

Figure S2. X-ray diffractogram of bulk MoS_2 powder and CE-MoS_2. The reflections are absent in CE-MoS_2. This confirms the high degree of exfoliation in the CE-MoS_2 precursor.

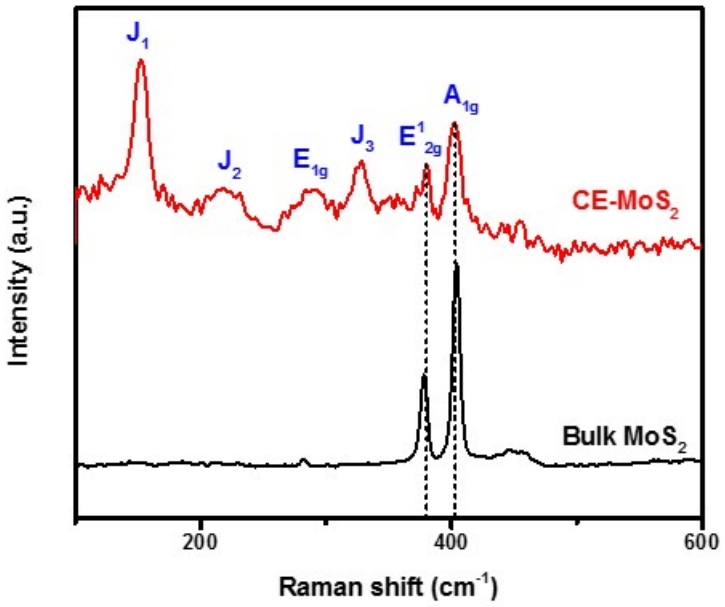

Figure S3. Raman spectra of bulk MoS_2 and CE-MoS_2. For the CE-MoS_2, the A^1_g mode blueshifts by approximately 2.5 cm^{-1}, while E^1_{2g} mode redshifts by approximately 1.3 cm^{-1}, suggesting that CE-MoS_2 is ulatrathin after exfoliation. Besides, more vibrational modes are detected, indicating the successful exfoliation.

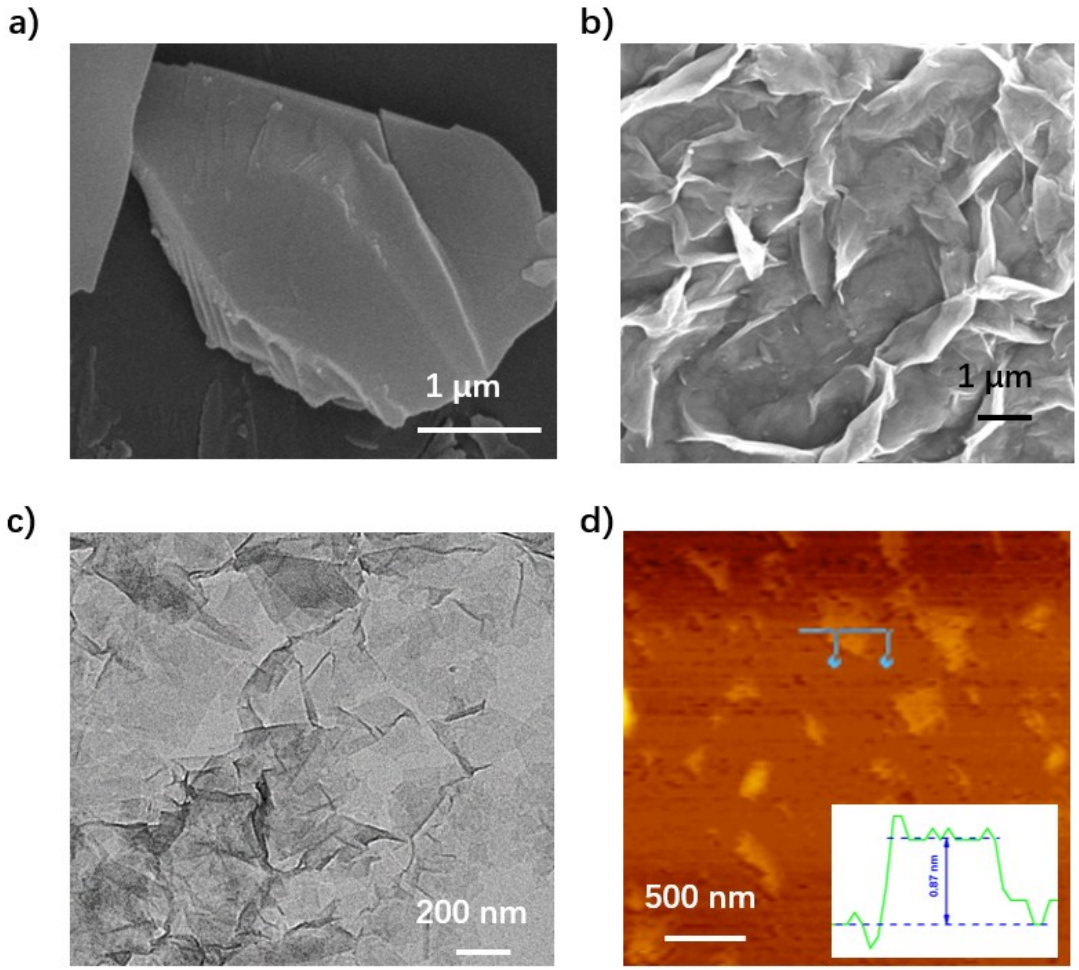

Figure S4. a) SEM image of bulk MoS_2. b) SEM c) TEM, and d) AFM images of CE-MoS_2.

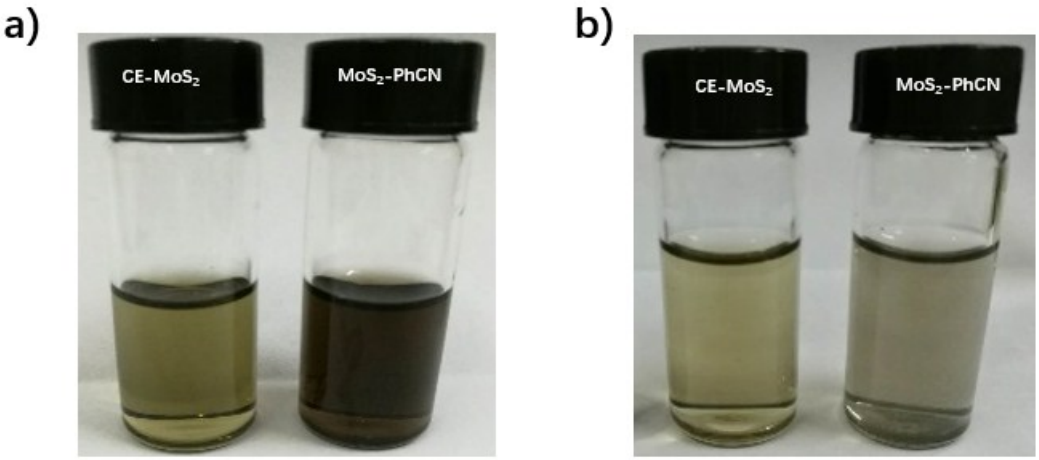

Figure S5. Photography of CE-MoS_2 and MoS_2-PhCN dispersions in a) DMF and b) deionized water, respectively.

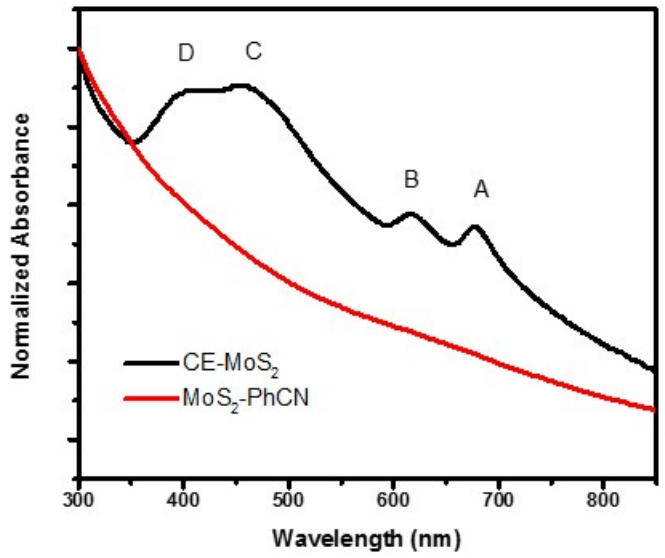

Figure S6. Normalized UV-vis spectra of CE-MoS_2 and MoS_2-PhCN.

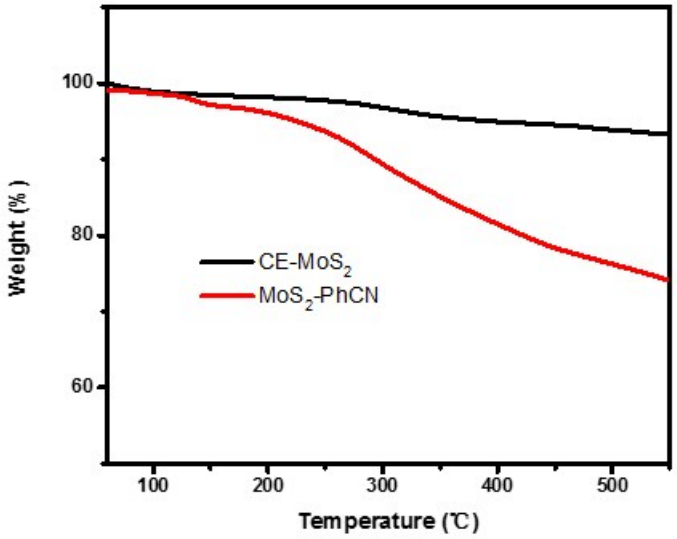

Figure S7. TGA profiles of CE-MoS_2 and MoS_2-PhCN. The difference in the weight loss between CE-MoS_2 and MoS_2-CN is associated to degradation of the 4-cyanobenzyl functional groups.

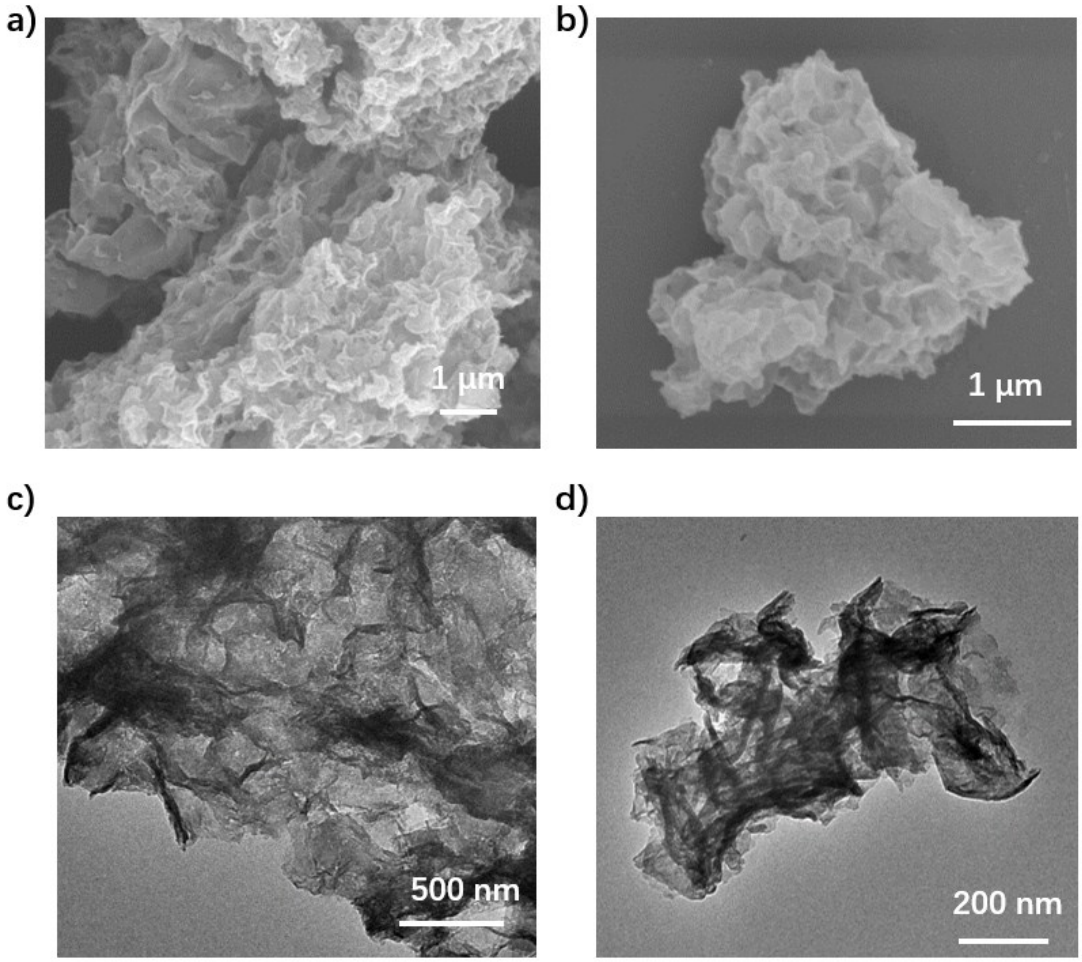

Figure S8. a), b) SEM and c), d) TEM images of MoS_2-PhCN.

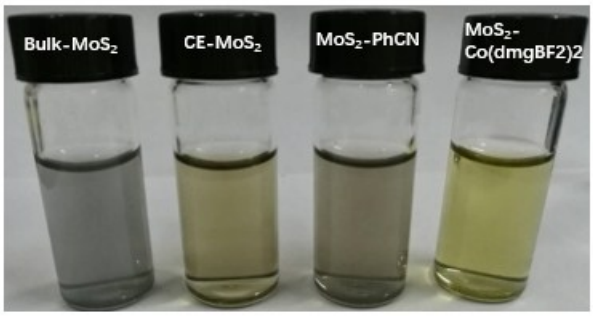

Figure S9. Photography of bulk MoS_2, CE-MoS_2, MoS_2-PhCN and MoS_2-Co($dmgBF_2$)$_2$ dispersions in deionized water.

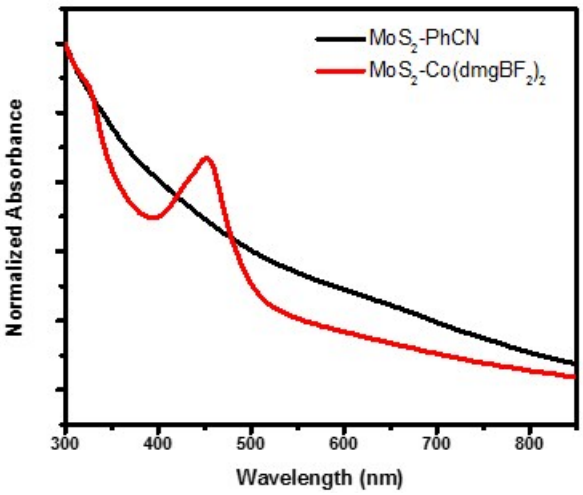

Figure S10. Normalized UV-vis spectra of MoS_2-PhCN and MoS_2-Co($dmgBF_2$)$_2$.

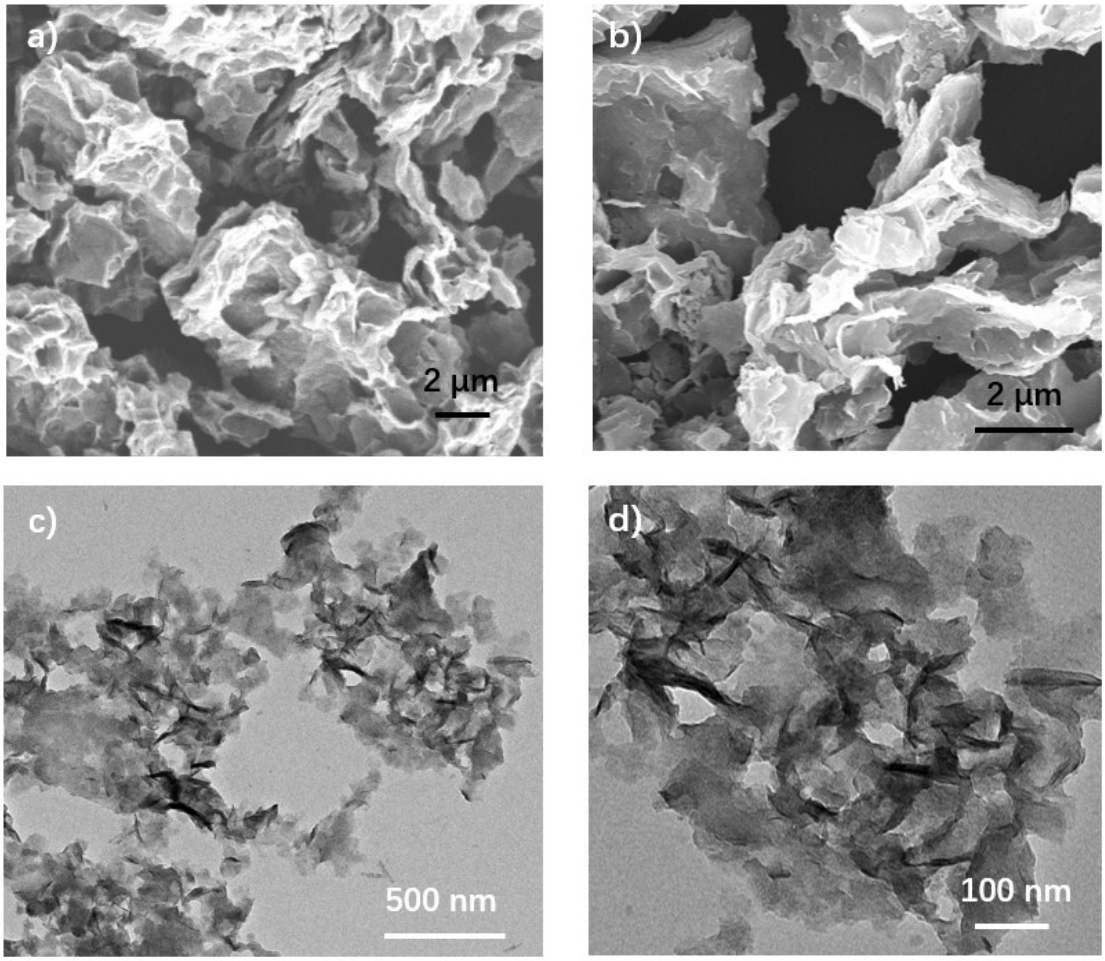

Figure S11. a), b) SEM and c), d) TEM images of MoS_2-Co($dmgBF_2$)$_2$.

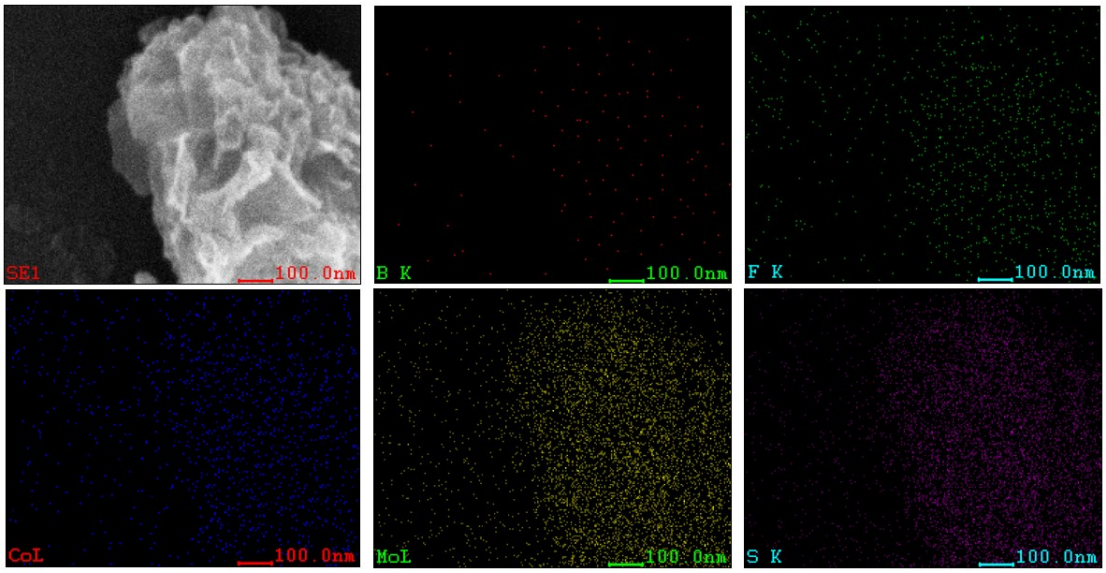

Figure S12. SEM images and elemental mapping for MoS_2-$Co(dmgBF_2)_2$, revealing the uniform distribution of Co in the MoS_2-PhCN nanosheets.

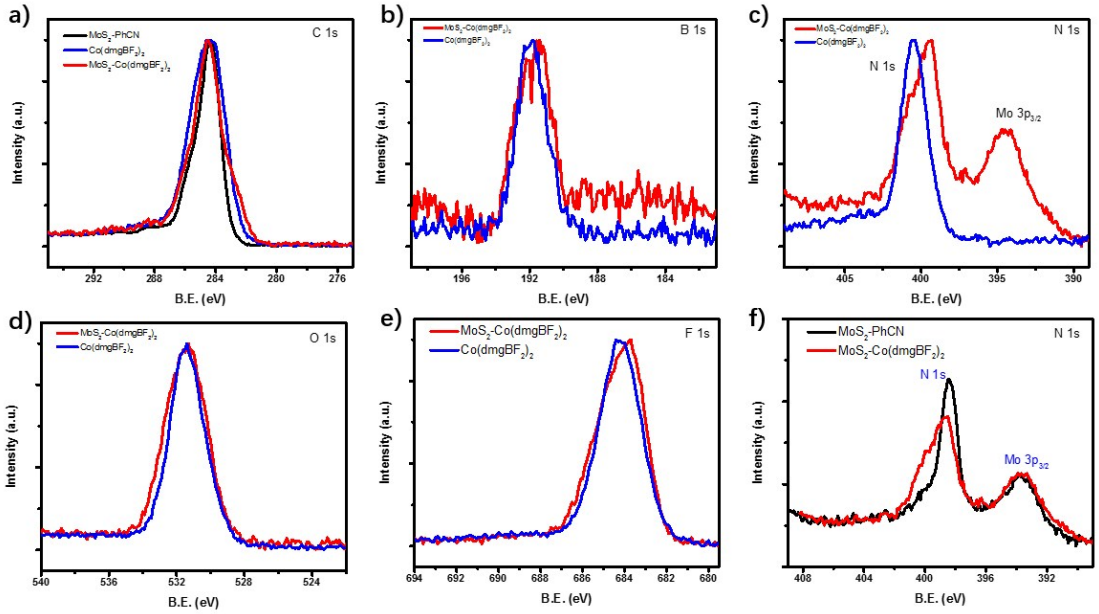

Figure S13. XPS spectra of the samples.

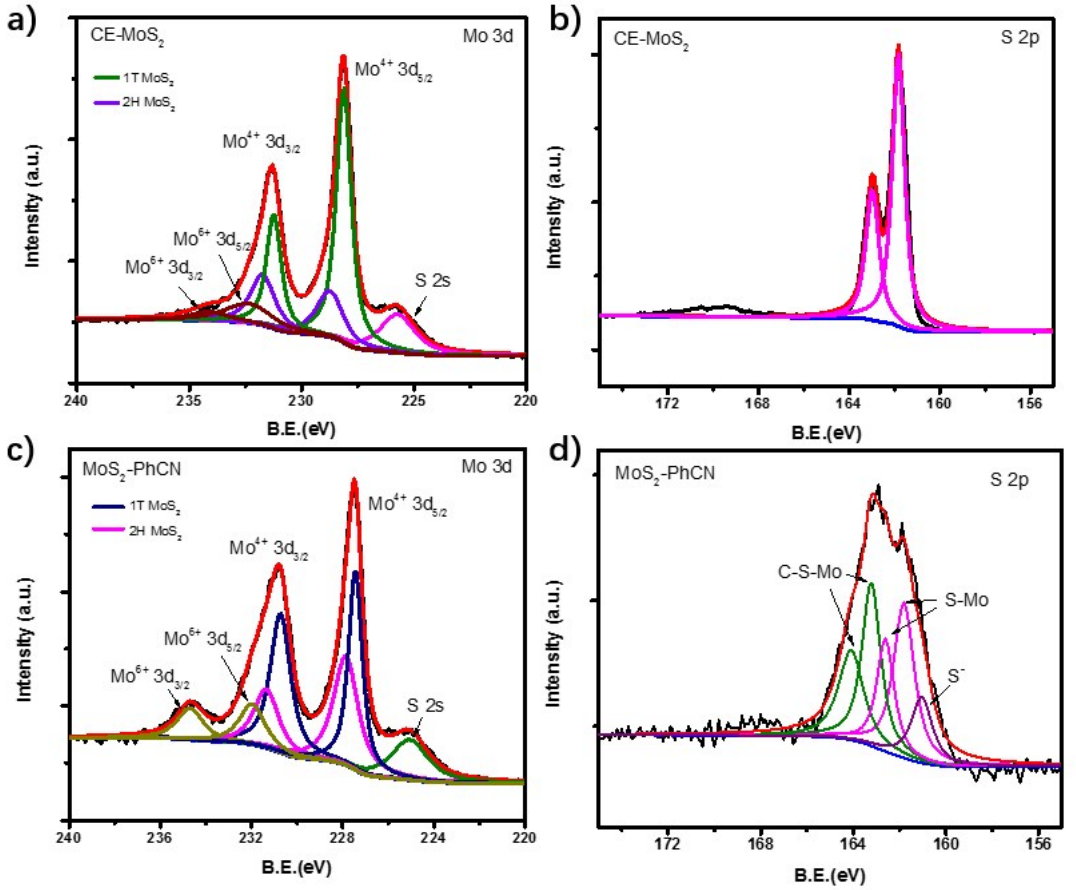

Figure S14. a) Mo 3d, b) S 2p spectra of CE-MoS_2. c) a) Mo 3d, b) S 2p spectra of MoS_2-PhCN. The peaks of Mo^{4+} $3d_{5/2}$ and $3d_{3/2}$ are split into the 1T phase and 2H phase, suggesting the presence of both phases. The 2H/1T ratio of the CE-MoS_2 and the MoS_2-PhCN is slightly different due to functionalization and structural rearrangement. Peaks at binding energies of 234.9 and 232.2 eV can be ascribed to surface-oxidized MoO_3.

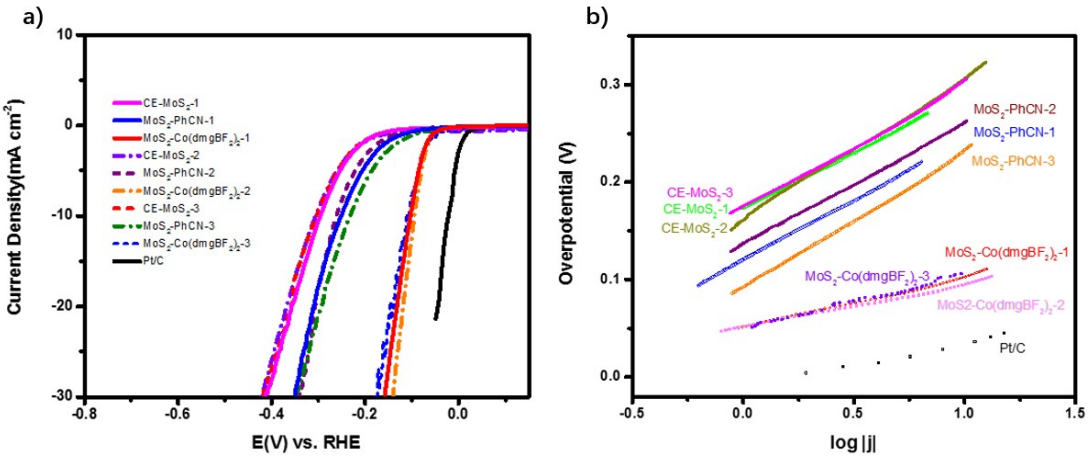

Figure S15. (a) Polarization curves and (b) corresponding Tafel plots of repeating samples.

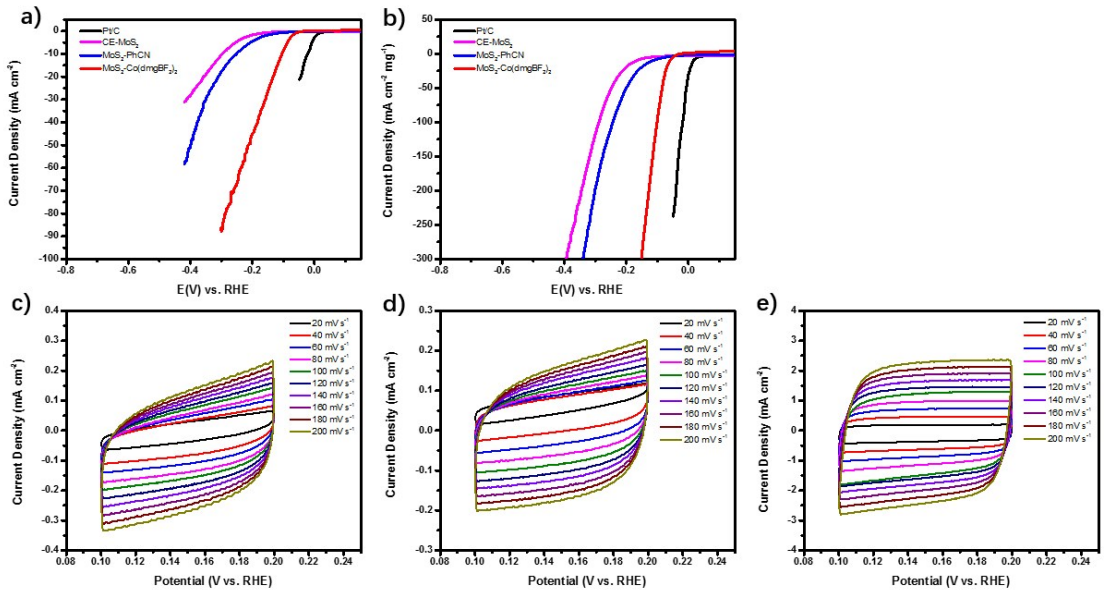

Figure S16. a) and b) Polarization curves, Cyclic voltammograms (CV) curves of c) CE-MoS_2, d) MoS_2-PhCN and e) MoS_2-Co($dmgBF_2$)$_2$.

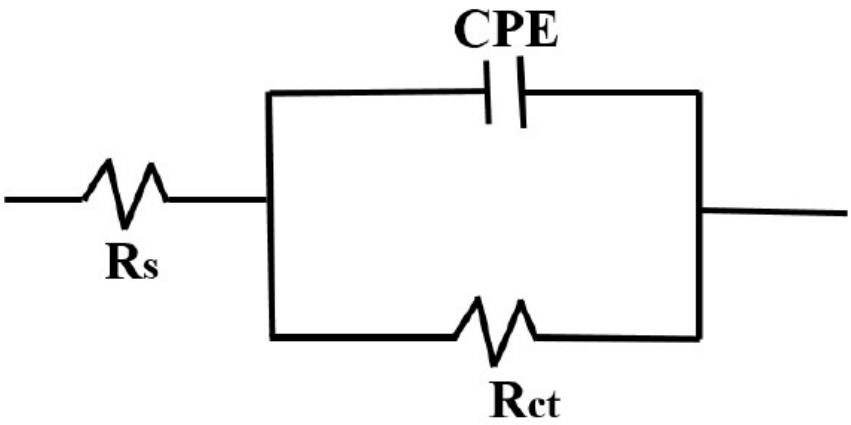

Figure S17. Equivalent circuit used for fitting of EIS data. R_s is the overall series resistance and R_{ct} is the charge transfer resistance, R_{ct} value generally varies inversely to the electrocatalytic activity. CPE is the constant phase angle element, which represents the double layer capacitance of solid electrode in the real-world situation.

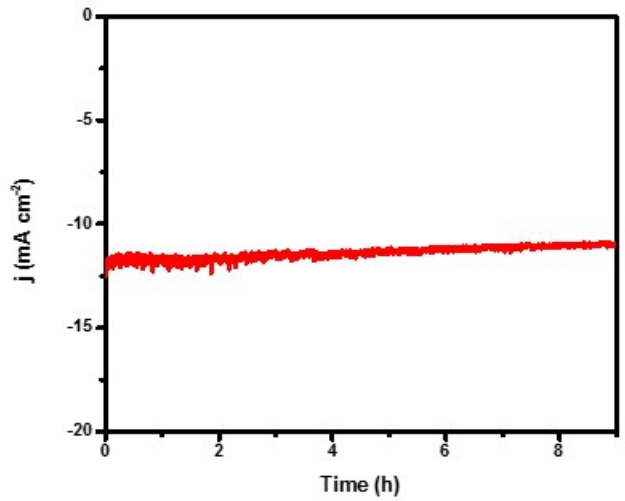

Figure S18. Current density-time (I-t) curve of MoS_2-$Co(dmgBF_2)_2$ under static overpotential of 110 mV for 9 h.

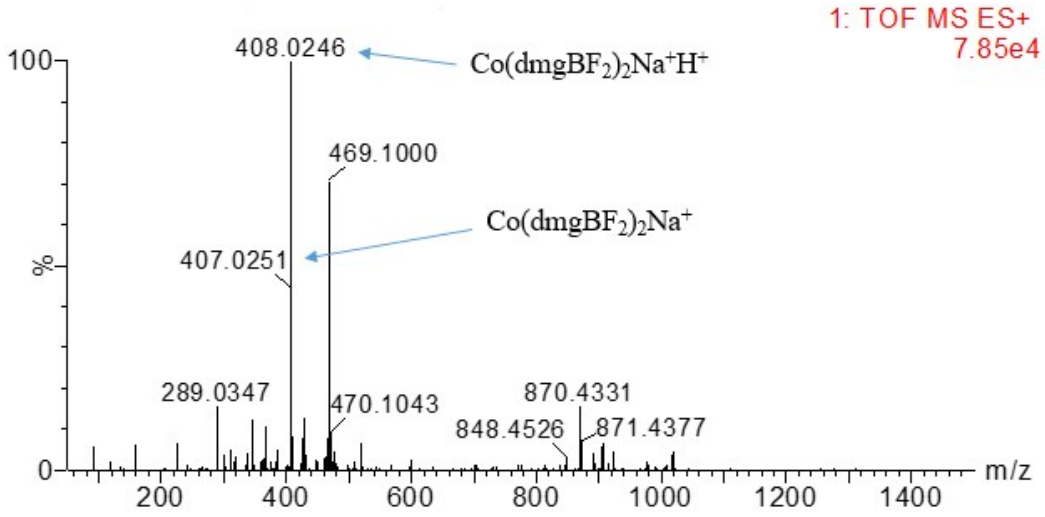

Figure S19. Mass spectra of $Co(dmgBF_2)_2$.

Table S1. Estimation of the atoms content in MoS_2-PhCN and MoS_2-$Co(dmgBF_2)_2$. The results were calculated according to the spectral intensity ratios of XPS.

Sample	Atom Conc %						
	Mo	S	C	N	Co	B	F
$Co(dmgBF_2)_2$	/	/	61.23	15.73	2.63	8.25	12.14
MoS_2-PhCN	3.01	6.10	83.81	7.08	/	/	/
MoS_2-$Co(dmgBF_2)_2$	3.71	7.53	66.49	9.64	1.58	5.05	6.01

Coordination percent of $Co(dmgBF_2)_2$ on the MoS_2-PhCN = $Conc_{Co}/(Conc_N-4*Conc_{Co})*100\%$

Table S2. Determination of Mo, S and Co ratio in MoS_2-PhCN and MoS_2-$Co(dmgBF_2)_2$. The results were determined by ICP-AES analysis.

Sample	Content wt %			Mole ratio
	Mo	S	Co	$n_{Mo} : n_S : n_{Co}$

MoS_2-PhCN	27.27%	18.62%	0.0039%	1 : 2.04 : 0
MoS_2-Co($dmgBF_2$)$_2$	25.55%	15.17%	3.78%	1 : 1.79 : 0.24

Table S3. Comparison of HER performance in acidic media for MoS_2-Co($dmgBF_2$)$_2$ with selected state-of-the-art MoS_2-based HER electrocatalysts.

Catalysts	Overpotential at 10 mA cm^{-2} (mV vs. RHE)	Tafel slope (mV dec^{-1})	Exchange current density (μA cm^{-2})	Electrochemical double-layer Capacitances (Cdl) (mF cm^{-2})	Ref
MoS_2	322	91	3.7	4.7	*Adv. Funct. Mater.*, 2017, **27**, 1602699
CoS_2@MoS_2	290	86	5.8	6.0	*Adv. Funct. Mater.*, 2017, **27**, 1602699
P-1T-MoS_2	153	43	15.8	63.1	*J. Am. Chem. Soc.*, 2016, **138**, 7965
Ni-Co-MoS_2	155	51	9.1	11.7	*Adv. Mater.*, 2016, **28**, 9006
C_3N_4−MoS_2	278 (at 5 mA cm-2)	88	n/a	n/a	*ACS Appl. Mater. Interfaces*, 2017, **9**, 10664
HF-MoSP-800	108	76	n/a	n/a	*Nanoscale*, 2016, **8**, 11052
defective O-doped MoS_2	180	55	12.6	37.7	*J. Am. Chem. Soc.*, 2013, **135**, 17881
MoS_2/RGO hybrid	150	41	n/a	n/a	*J. Am. Chem. Soc.*, 2011, **133**, 7296
amorphous MoS_xCl_y	160	46	n/a	12.8	*Energy Environ. Sci.*, 2015, **8**, 862
Co-doped MoS_2/nitrogenated graphene	170	59	23.6	n/a	*Mater. Sci. Eng. B*, 2016, **212**, 30
Co-MoS_2-C	135	50	30.1	10.4	*ACS Appl. Mater. Interfaces.*, 2015, **7**, 27242
MoS_2@TiO_2	340	81	n/a	n/a	*ACS Appl. Mater. Interfaces.*, 2016, **8**, 26794
MoS_2-Co($dmgBF_2$)$_2$	103	45	64.5	11.5	This work

Table S4. Over-potential and Tafel slope of repeating samples.

Samples	Ponset (mV)	Mean (mV)	Standard Deviation	Tafel slope (mV dec^{-1})	Mean (mV)	Standard Deviation
CE-MoS_2-1	132			113.54		
CE-MoS_2-2	146	138	5.79	130.13	120.62	8.56
CE-MoS_2-3	137			118.18		
MoS_2-PhCN-1	81			119.68		
MoS_2-PhCN-2	94	84	6.9	119.89	123.96	7.24
MoS_2-PhCN-3	78			132.32		
MoS_2-Co($dmgBF_2$)$_2$-1	41			44.77		
MoS_2-Co($dmgBF_2$)$_2$-2	42	42	1.2	39.18	42.59	2.44
MoS_2-Co($dmgBF_2$)$_2$-3	44			43.83		

Table S5. R_{ct} values of CE-MoS_2, MoS_2-PhCN and MoS_2-Co($dmgBF_2$)$_2$.

Sample	R_{ct}
CE-MoS_2	1247
MoS_2-PhCN	880
MoS_2-Co($dmgBF_2$)$_2$	443

From the above table, we can see that MoS_2-Co($dmgBF_2$)$_2$ shows the smallest value of R_{ct}, which exhibits the fastest electron transfer properties among the samples.